Unraveling the Molecular Origin of Prey-Wrapping Spider Silk's Unique Mechanical Properties and Assembly Process Using NMR

*Kevin Chalek[a], David Onofrei[a], Julian E. Aldana[a], Hannah Johnson[a], Dillan Stengel[a], Andy T. Chau[a], Anikin Rae Domingo[a], Erik Alcala[a], Esther Tsui[a], Francisco Botello[a], Ashana Soni[a], Bennett Addison[b] and Gregory P. Holland[a]**

a. Department of Chemistry and Biochemistry, San Diego State University, San Diego, CA, 92181-1030, USA

b. Renewable Resources and Enabling Sciences Center, National Renewable Energy Laboratory, Golden, CO, USA

*E-mail: gholland@sdsu.edu

Keywords

NMR Spectroscopy, Spider Silk, Mechanical Properties, Protein Structure, Fibers

ABSTRACT

Prey wrapping spider silk's unique mechanical properties are investigated confirming the silk's high degree of extensibility and superior toughness compared to other types of spider silk. For the first time, the pre-spinning dope phase is studied in isotope-enriched intact aciniform (AC) silk glands using solution NMR that reveals a combination of α-helical domains linked by disordered random coil chains consistent with previously proposed "beads-on-a-string" models. The model is further refined through the AlphaFold2 protein structure prediction tool that is fed native AC silk protein sequences. Finally, extensive magic angle spinning (MAS) solid-state (SS)

NMR data for isotopically-enriched fibers is used to refine the structural model for AC silk from two species, *A. aurantia* and *A. argentata*. The SSNMR data shows that the AC silk fibers are highly α-helical, coiled-coil in structure but, also exhibit significant β-sheet components that can be traced back to the Gly-rich disordered linker regions in the pre-spinning dope phase that are converted to β-sheet structures during fiber formation. This combination of mechanical and structural characterization enhances our understanding of AC silk's liquid-to-solid transition and structure-mechanics relationship. These prey wrap silk results and models will provide the basis for the design of biomimetic materials inspired by the AC spider silk system.

1. Introduction

The most extensively studied spider silk proteins are dragline, or Major Ampullate (MA) silk spidroins (MaSp), due to their ease of collection and study.[1-4] However, the toughest and finest silk amongst the seven different types of silk spiders produce is aciniform (AC) silk that spiders utilize to wrap prey, line their egg-cases and in some cases as web decoration (**Figure 1**).[1, 5-7] Although AC silk's superior mechanical properties have been demonstrated in a few studies,[6, 8] they are far from established and still require further investigation because of the significant challenges associated with measuring the mechanical properties of sub-micron scale fibers. In addition, the conformational and hierarchical structure of this unique

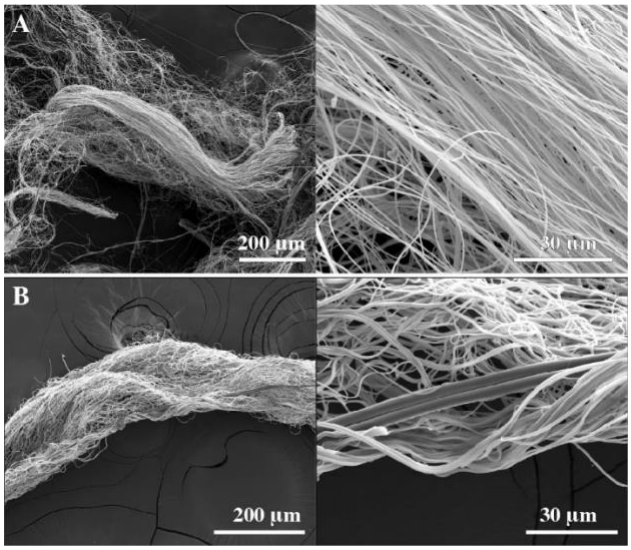

Figure 1. SEM image of (A) *A. aurantia* AC silk collected by vibration-induced attack wrapping and (B) *A. argentata* AC silk utilized in zig-zag web decoration where it is wrapped around MA silk. AC silk is the thinnest spider silk with a fiber diameter ~ 0.5 µm.

biopolymer has only recently begun to be elucidated by our lab using magic angle spinning (MAS) Solid-State NMR (SSNMR) and here this structural characterization is further developed.[9, 10] The mechanical properties of spider silk, as well as their numerous potential industrial and biomedical applications, drives most of the research on silk biopolymer fibers. The key to unlocking this potential lies in connecting the molecular landscape with the macroscopic tensile properties for all types of spider silk, but particularly for AC silk because of its exceptional toughness. There is also very limited information available regarding the native AC silk protein conformational state prior to fiber formation, as stored within the gland environment. This native gland state is further explored in the present work with solution NMR on isotopically enriched native AC glands.

The protein aciniform spidroin 1 (AcSp1) is the primary component of spider prey-wrapping fibers. *A. argentata* AcSp1 is made up of 4479 total residues, with 20 iterated, nearly identical repeats of the wrapping (W) subunit composed of primarily α-helical domains and a β-sheet forming linker portion flanked by N- and C- terminal regions (**Figure S1**).[9-11] The structure of native AcSp1 prior to spinning has been investigated with CD and Raman spectroscopy and shown to exhibit α-helical content in the gland environment.[12-15] This is in stark contrast with MaSp proteins that are highly dynamic, predominantly random coil in the MA gland environment displaying backbone dynamics analogous to an intrinsically disordered protein (IDP).[16-21] Solution NMR studies of a small recombinant AcSp "bead" component agree with the predominantly α-helical conformation for the AcSp in solution.[22-24] In the present study, we investigate intact isotope-enriched AC silk glands with solution NMR for the first time providing new data to understand the native pre-spinning state of AC silk proteins.

We have previously shown that *A. argentata* AcSp1 within freshly-spun AC silk fibers is predominantly α-helical, exhibiting a coiled-coil conformational structure with a low β-sheet content (~15%) compared to MA silk.[9] The high degree of extensibility of AC fibers is likely a result of α-helical portions together with contributions from retained random coil regions. In addition to its toughness, AC silk fibers undergo matted cross-linking upon exposure to moisture. This unique water-induced process converts the extensible α-helix-rich fiber into a rigidified mat with increased β-sheet content.[10] To gain a more complete molecular view of AC silks fiber's conformational structure, and to better understand its unique mechanical properties, we have produced several $^{13}C/^{15}N$-isotope enriched silks and characterized them with solution and SSNMR to determine secondary structure based on chemical shifts both prior to and following fibrillization. To build more complete structural models, characterization by NMR is further supported by structural models predicted with AlphaFold2 from AC silk protein sequences.[25, 26] By combining mechanical tensile testing, solution NMR, and solid-state NMR together with the AlphaFold2 structure prediction, a holistic view of AC silk formation and mechanical performance is gained. Structural correlations can be made across the liquid-to-solid transition and structural information in fibers can be rationalized in the context of mechanical performance. Overall, this work greatly expounds upon our molecular and mechanical understanding of the AC silk system for improved biomimetics in future work.

2. Results and Discussion

2.1 Mechanical Testing of Spider Silk Fibers

Accurately measuring the mechanical properties of spider silks and finding correlations to the underlying molecular structures is a key step to generating synthetic silk fibers with tunable properties. Spiders produce up to seven different types of silk, however, the majority of

the literature has focused on MA silk because it can be forcibly extracted from spiders. MA silk has incredible strength for a biological polymer compared to man-made materials[27, 28] but, prey wrapping silks exhibit moderate strength (~600-700 MPa) and high extensibility (~50-80%) making them the toughest of the spider silks.[6, 8] Here, the tensile properties of MA silk fibers for several spider species and AC silk from *A. argentata* were measured (**Figure 2/Table 1**). Our measured MA silks are well within the limits of published values. Humidity, age, anesthesia, reeling speed, and spider condition (gravid, time since last feeding) and many other variables have been shown to result in fibers of varying mechanical properties, even for spiders of the same species and sometimes even among individual spiders.[29-32] Nevertheless our results find the general trends that have been published in the literature to hold true for MA silk, *N. clavipes* and *A. argentata* MA silks are slightly stronger than *L. hesperus* while, the latter is the most extensible.[33]

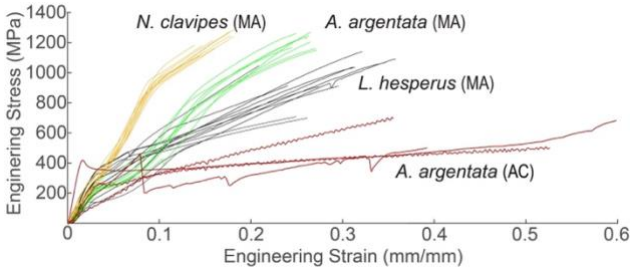

Figure 2. Stess/strain curves for MA silk fibers collected from three different species of spider and AC silk from *A. argentata*. AC silk exhibits moderate strength with greater extensibility and toughness compared to MA silks.

Table 1. Mechanical properties of Different types of spider silk fibers and their measured strength, extensibility, toughness and diameter.

Species	Strength(MPa) Engineering/ True	Extensibility(mm/mm) True/Engineering	Toughness (MJ/m^2)	Fiber Diameter (μm)
L. Hesperus (MA) N = 24	1008±267/1280±284	34±4%/29±4%	164±82	2.54±0.15
N. clavipes (MA) N = 28	1146±188/1340±194	17±3%/16±3%	113±33	3.59±0.2
A. argentata (MA) N = 15	1204±104/1524±106	27±2%/24±2%	177±15	1.84±0.84
A. argentata (AC) N=3	592±98	46%±12%	179±53	0.50

AC silk presents the greatest challenge for mechanical measurement due to the extremely small cross-sectional diameter (~0.5 μm) and the difficulty in separating the swath of silk (see methods) into individual fibers. Multiple breaks are often observed in the stress/strain curves of AC silk fibers making single fiber measurements difficult. Nonetheless, a number of successful measurements were made that agree with previously published data[6, 8] and illustrate that AC silk exhibits a higher extensibility and toughness compared to the MA silks. Despite lacking the same ultimate strength of the MA silk, AC silk nevertheless maintains moderate strength and, notably, exhibits the greatest extensibility and toughness of all the measured spider silks.

2.2. AlphaFold Structural Model of AcSp1

The previous hierarchical molecular protein model for AcSp1 in solution was described as "beads-on-a-string" system in which the "bead" is a 5-helix bundle and the "string" is a disordered linker domain rich in Ser, Ala and Gly.[13] When the soluble protein dope is spun into an insoluble fiber, the "bead" regions remain highly helical while the string/linker regions form pleated β-sheet subunits in AC silk fibers.[9] However, the solution-state structure of the AcSp protein is based on NMR work on isolated and purified recombinant protein at low concentration and thus, may not fully represent the nuanced structure in the intact gland at native protein concentration. To investigate the molecular structure of a larger protein with multiple wrapping units in higher concentration, the AcSp1 solution phase structure was refined using AlphaFold2, an artificial intelligence program developed by DeepMind that can predict a given protein's 3D structure using the primary amino acid sequence as the input.[25, 26] The results of the AlphaFold2 prediction for the entire *A. argentata* AcSp1 (**Figure 3**) are consistent with the "beads-on-a-string" model, but refines the model into seven separate helices in the "bead" with each helix

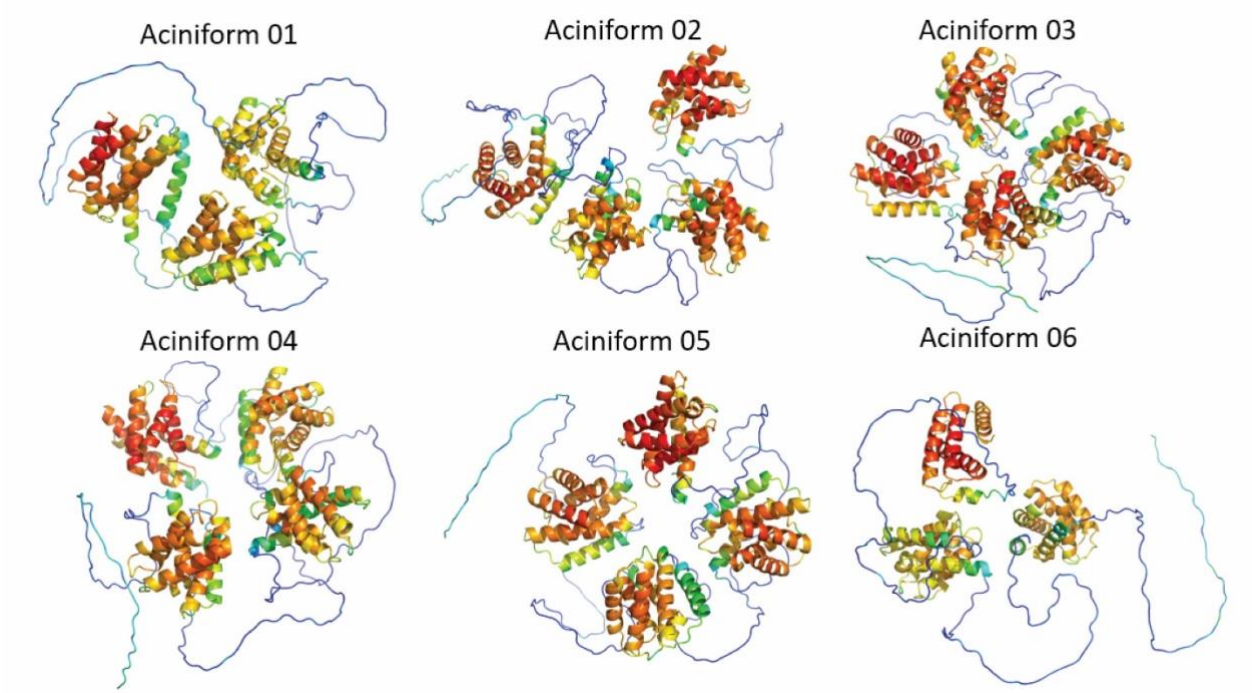

Figure 3. The structure of *A. argentata* AcSp1 predicted with AlphaFold2. The entire sequence (**Figure S1**) was split into 6 portions for structural predictions to look at the complete sequence piecemeal. The "beads-on-a-string" model is refined into seven separate helices in the "bead" with each helix connected by short, unstructured, sequences. Each "bead" is then connected by longer, unstructured "strings". Red is high confidence (~80) and blue is low confidence (~20). Helical bundles attained confidence scores ranging from 58-80, while linkers consistently scored from 22-27 in all 6 structure predictions.

connected by short, unstructured, random coil linkers. The primarily α-helical "beads" are connected by long unstructured, random coil "strings" that are rich in Ser/Ala/Gly. β-sheet conformations are completely absent in the AlphaFold structures, but these unstructured "string" regions were shown to have portions that assemble into β-sheets in solid fibers by SSNMR (see below).[9] Six different structural models were generated with AlphaFold (**Figure 3**) to evaluate the entire AcSp1 sequence (**Figure S1**) piecemeal. The results are extremely similar across the

Table 2: Secondary structure quantification based on DSSP analysis of structures predicted from the *A. argentata* sequence using AlphaFold2. See SI for complete table (**Table S1**).

Amino Acid	Ala	Ser	Val	Leu	Gly	Thr	Pro	Phe
α-helix	64%	52%	59%	81%	23%	45%	4%	39%

entire sequence confirming the α-helical "beads-on-a-string" model. The percentages of each residue assigned an α-helix secondary structure based on the AlphaFold generated structural model and DSSP quantification is presented in **Table 2**. **Table S2** shows the complete DSSP secondary structure quantification, showing that 52% of the AcSp1 protein is in an α-helical secondary structure in solution, while 36% is unstructured. The remaining predicted secondary structures are mostly β-turn contributions for Gly.

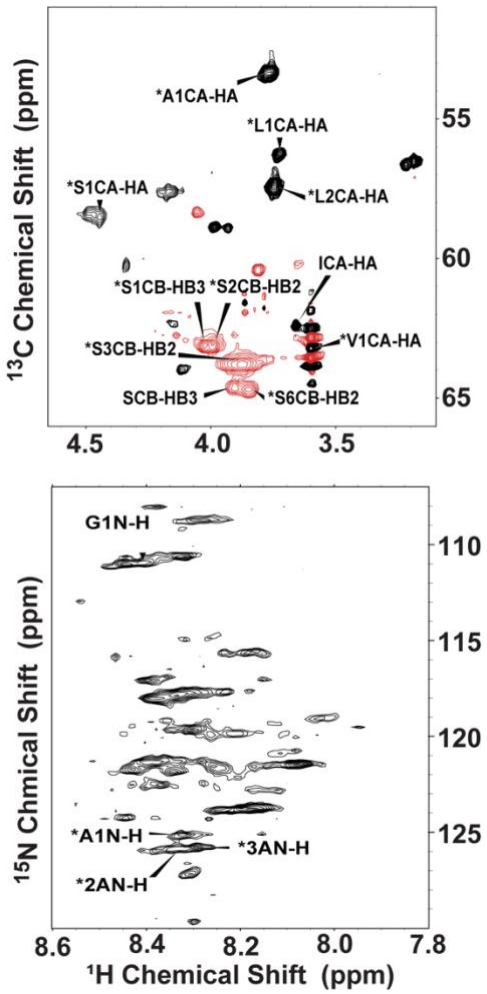

Figure 4. ^{13}C (top) and ^{15}N (bottom) solution NMR HSQC spectrum of U-[^{13}C/^{15}N]-Val-labeled *A. aurantia* AC glands. Assignments are based on expected values for each amino acid and comparison to known chemical shifts.

2.2 Solution NMR of Intact AC Silk Glands

Previous solution NMR work has shown that recombinantly expressed W subunits of the AcSp silk protein form α-helical bundles connected by loose linker regions,[22-24] and these results are highly supported by our AlphaFold predictions described above. The next critical step in understanding the formation of AC silk fibers was to investigate whether or not the proposed conformational state of the solubilized AC silk protein resembles the native protein structure within intact glands. For example, are the "beads" indeed α-helical as the AlphaFold model predicts and are the string domains, truly unstructured random coils? We endeavored to study the native silk protein by dissecting the AC glands and performing solution NMR experiments for the first time to investigate the AC silk proteins in entirety and at native

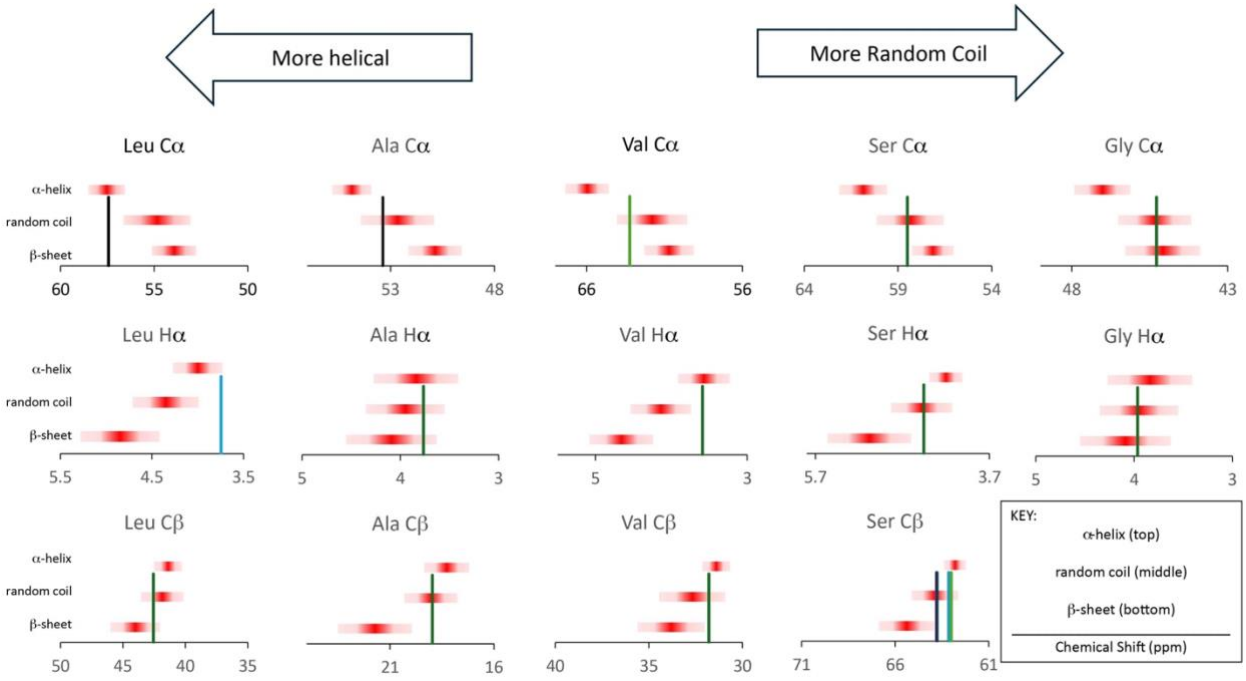

Figure 5. Comparing the chemical shifts of five assigned amino acids from the 2D ^{13}C-HSQC spectra of isotopically labeled AC glands with their respective ranges for three types of secondary structure: α-helix, β-sheet, and random coil.

concentration within intact glands while, utilizing the recombinant W subunit as a point of while utilizing the recombinant W-unit as a point of reference.

Solution NMR 2D ^{13}C- and ^{15}N-HSQC spectra were collected for four isotopically labeled AC silk gland samples excised from *A. aurantia* spiders to characterize AC silk protein secondary structure. The solution NMR spectra for U-[^{13}C/^{15}N]-Val labeled AC glands is shown in **Figure 4** (^{13}C data for Ala-, Leu- and Thr-labeled AC glands see **Figure S2**). Chemical shift data is reported from ^{13}C-HSQC spectra for amino acids that had confident assignments (**Table S2**). While there are many unassigned resonances due to high spectral overlap, five of the most abundant amino acids in AC silk: Ser, Ala, Val, Leu and Gly could be assigned in multiple spectra produced with different isotope labeling schemes. The main assumption is that the assigned resonances correspond with the secondary structure associated with that range based on the values from Wang and Jardetzky.[34]

Assignments of individual Cα, Cβ and Hα resonances based on the 2D ^{13}C-HSQC spectra for U-[^{13}C/^{15}N]-labeled AC glands are compared to known values for different secondary structures (**Table S2**, **Figure 5**). To aid our initial assignments, we took advantage of spectral editing (clearly identifying Cβ among Cα), the unique case of the Cβ of Ser (which shows up at higher ppm than the Cα) the unique assignment of Gly, and finally close comparison to the work of Rainey's on recombinant AC proteins.[12-15] Of the assigned resonances, the Cα, Cβ, and Hα for Leu fall squarely in the α-helical region, Ala and Val lean towards their α-helical chemical shift range, and Gly falls very close to the expected value for a random coil. Ser aligns mainly on random coil for Cα and Hα, although several peaks identified for Ser Cβ are shifted towards the α-helical conformation. These solution NMR results are consistent with the AlphaFold2 structural model for AcSp1 where DSSP-determined α-helical content (**Table 2**) tracks with the observed conformational dependent ^{13}C and ^{1}H NMR chemical shifts. The highest α-helical content for any amino acid from AlphaFold2 model was 81% for Leu and solution NMR shows this amino acid to be the most α-helical (**Figure 5**). Ala and Val are the next most α-helical in the structural model (64 and 59%) and NMR shows that they lean towards α-helical shifts. Ser was a bit more ambiguous with the Cα and Hα indicating RC while, multiple Cβ fell in the α-helical range. The latter may not be too surprising since Ser is nearly equally present in α-helical (52%) and disordered domains. Finally, Gly fell squarely on random coil which is consistent with its dominant presence in string domains that are unstructured with the lowest (26%) α-helical content of any amino acid in the AlphaFold model.

Despite the emergence of some apparent α-helical structure, it is noteworthy that the chemical shift dispersion of the backbone amide protons is extremely small (<1ppm) as seen in **Figure 4** (and ^{15}N data for Ala- and Thr-labled glands; see **Figure S3).** Low ^{1}H chemical shift

dispersion is one of the first indicators that a protein is unstructured akin to an IDP.[35] By comparison, the recombinant W subunit structure has an amide ^{1}H dispersion >3ppm.[13] This suggests that while α-helices are abundant in the gland supporting the proposed model, there are a significant amount of unstructured, random coil domains than are not represented in the recombinantly expressed variant. This leads us to conclude that the string domains are completely unstructured which is supported by Gly's highly abundant presence in this domain and the determination that it displays the most random coil conformation by solution NMR for AC glands. It is stressed that these native AC gland results are in the early stages and further 2D/3D solution NMR experiments for native AC glands are expected to provide residue-specific assignments for determination of sequence specific structural propensity. Work that is ongoing in the lab. Nonetheless, the general trends observed in solution NMR are consistent with a combination of α-helical and random coil structure in the AC gland where the chemical shift trends track with α-helical propensity from the AlphaFold model (**Table 2**).

2.3 SSNMR of *A. argentata* AC Silks

Our previous solid-state NMR characterization of native as-spun *A. argentata* prey wrapping silks focused primarily on Ala, Ser, and Val residues. Our results supported an AC silk fiber rich in α-helices for the bead regions, with substantial disorder and minor β-sheets derived from the Ala/Ser/Gly-rich linker domains, resulting in a hybrid

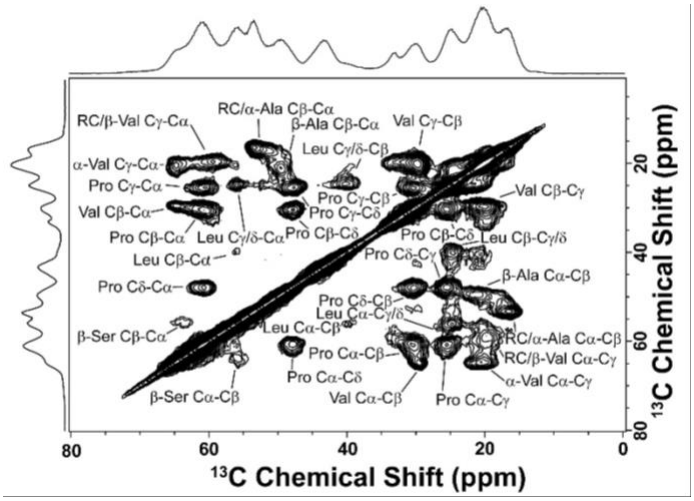

Figure 6. 2D ^{13}C-^{13}C through-space correlation CORD SSNMR experiment for *A. argentata* prey-wrap silk where the spider was fed a U-[^{13}C/^{15}N]-enriched solution of Val, Ala, Leu, and Pro. This experiment was collected with a mixing time of 50 ms to observe intramolecular dipolar contacts.

coiled-coil α-helical / β-sheet fiber.[9] Here, we further study the native structure of freshly spun prey wrapping silks with additional investigation into Leu, Pro, Gly, and Phe/Tyr. ^{13}C-^{13}C SSNMR correlation experiments were conducted for the U-[^{13}C/^{15}N]-enriched Val, Ala, Leu, and Pro (VALP) AC silk fibers to investigate secondary structure. First, a CORD spectrum was collected (**Figure 6**) that shows dipolar correlations through space. CORD sequences are used to drive ^{13}C-^{13}C spin diffusion in a broad frequency range, giving rise to a uniform distribution of cross peak intensities across the entire spectrum.[36] Then, the refocused DQ/SQ INADEQUATE experiment was performed to show correlations through a single bond (**Figure 7**). The Cα-CO correlations were the focus of the INADEQUATE experiment. These correlations were then extracted to compare experimental chemical shifts with literature values to determine secondary structure (**Tables 3 and 4**).

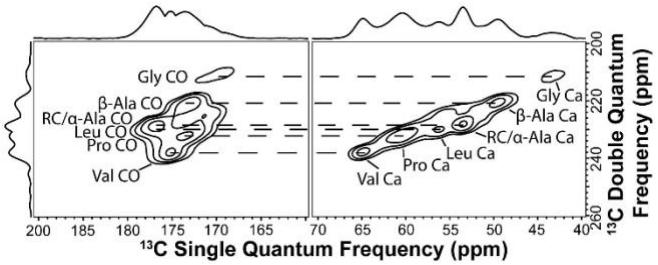

Figure 7. ^{13}C-^{13}C DQ/SQ through-bond correlation INADEQUATE experiment for *A. argentata* prey-wrap silk where the spider was fed a U-[^{13}C/^{15}N]-enriched solution of Val, Ala, Leu, and Pro. This experiment shows correlations through a single bond. This is zoomed in on the regions showing correlations between Cα and CO. The INADEQUATE was used to extract CO chemical shifts.

Proline

While AcSp1 lacks the easily observable repetitive motifs common in MaSp proteins, the repeating nature of the W subunit allows us to examine amino acids present in a greater variety

Table 3. Pro ^{13}C SSNMR chemical shifts (ppm from TMS) for *A. argentata* AC silk compared to *L. hesperus* and *A. aurantia* MA silks and other biopolymers with known secondary structures and the random coil conformation (RC).[37-40, 42]

Residue	*A. argentata* AC	*L. hesperus* MA	*A. aurantia* MA	Elastin	Collagen	RC
Pro Cα	60.7	60.7	60.7	60.0	58.2	61.9
Pro Cβ	30.1	30.0	30.5	29.9	29.1	30.6
Pro Cγ	25.4	24.9	25.4	24.6	24.1	25.6
Pro Cδ	47.6	47.6	47.5	48.2	47.1	48.3
Pro CO	174.1	174.0	174.8	171.8	173.9	174.1

of motifs. Proline, for example, is almost always in a VPT, GPS, or GPV motif outside of the terminal regions. The distinct Pro Cδ signal at 47.6 ppm in the 2D CORD experiment has clear through-space correlations with resonances at 60.7, 30.1, 25.7 and 174.1 ppm, corresponding to Pro Cα, Cβ, Cγ and CO, respectively (**see Figure 6** and **Table 3**). Further confidence is gained with slice selection of the 2D CORD to obtain a pseudo-1D spectrum of the signals close in space to Pro Cδ, containing ^{13}C isotropic chemical shifts for all Pro sites (**Figure S4**). Extracted Pro chemical shifts are compared to the biopolymers elastin and collagen with known secondary structures, along with the random coil conformation (**Table 3**).[37-40] These results are consistent with those previously obtained on ^{13}C -Pro labelled *A.aurantia* and *L. hesperus* dragline silk, where a GPGXX motif was determined to be similar in structure to elastin.[41-44] This elastin-like type-II β-turn formed by Pro containing motifs is correlated to spider silk's extensibility and could contribute to AC silk's significant extensibility and toughness (**Figure 2 and Table 1**).[45-47]

When compared to the DSSP secondary structure quantification in **Table S1**, a β-turn secondary structure is predicted to only occur 3% of the time for Pro. This is consistent with the argument that Pro-containing regions are unstructured in the gland and only form the elastin-like type II β-turn in the solidified fiber.

Leucine

In *A. argentata* AcSp1, Leu is predominantly present (81%) in the α-helical "bead" region of the repeating subunit (**Figure 3**, **Table 2**) with only ~7% of Leu found in the unstructured linker region of AlphaFold model (**Table S1**). Leu is positioned similarly to Val in

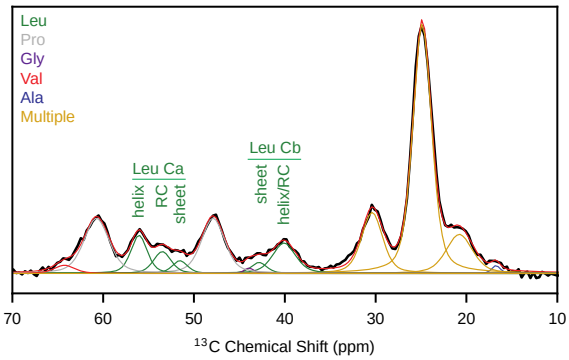

Figure 8. Leu slice (25 ppm) extracted from the 2D CORD (**Figure 6**) for *A. argentata* prey-wrap silk where the spider was fed a U-[^{13}C/^{15}N]-enriched solution of Val, Ala, Leu, and Pro. This Leu slice was used to quantify secondary structure through spectral fitting.

the primary protein sequence, and we previously found that Val is over 70% α-helical in the fiber[9], thus we anticipated a similar helical environment for Leu residues. Indeed, visual inspection of the 2D CORD (**Figure 6**) shows clear and predominant Leu Cα and Cβ intra-residue contacts with Leu Cγ/δ methyl carbons at 55/26 and 40/25 ppm that are consistent with a highly α-helical substructure (**Figure 6, Table 4**). For further clarity we extracted a 1D horizontal slice at 25 ppm, corresponding to Leu Cγ, Leu Cδ, Pro Cγ, and possibly β-sheet Ala Cβ (**Figure 8**), and spectral deconvolution of the corresponding Leu Cα and Cβ signals was

Table 4. ^{13}C SSNMR chemical shifts (ppm) for AC silk compared to known average shifts for specific secondary structures.[48] Leu, Gly and Phe chemical shifts are for *A. argentata*. Thr chemical shifts are for *A. aurantia*.

Residue	Experimental Shifts (ppm)	β-sheet	Random Coil	α-helix
Leu Cα	56.1	51.8	52.8	55.3
Leu Cβ	39.6	42.2	40.3	39.5
Leu CO	175.4	173.4	174.4	176.1
Gly Cα	43.5	43.2	43.3	44.7
Gly CO	170.1	170.1	171.8	173.3
Phe Cα	55.3/61.7	54.4	55.5	58.5
Phe Cβ	37.5/41.3	40.0	37.7	36.9
Phe CO	173.0	172.2	172.9	174.5
Tyr Cα		54.6	55.6	58.6
Tyr Cβ		39.1	37.0	36.1
Tyr CO		172.3	173.1	175.0
Thr Cα	59.2	59.1	59.5	63.4
Thr Cβ	67.0	68.4	67.5	66.2
Thr CO	172.6	171.6	172.5	173.9

applied to obtain a more quantitative understanding of Leu substructure. When fitting the Leu slice, multiple correlations must be considered corresponding to the signals expected from Leu, Pro, and Ala residues. Leu Cα is quite sensitive to protein secondary structure and indeed is composed of three main features centered at chemical shifts consistent with α-helical, random coil and β-sheet structures.[48] Deconvolution of the Leu Cα signal suggests that roughly 80% of all Leu adopts α-helix or random coil structure, 50% of which is truly helical and 30% random coil, and the remaining ~20% adopts a β-sheet configuration. These structural abundances for Leu are slightly lower in helical content and higher in random coil / β-sheet content relative to Val, as previously discovered.[9] While other residues like Ala Cα may also overlap in this region complicating confident interpretation, the Leu Cβ resonance is quite well resolved with limited overlap and also suggests 80% of Leu is either α-helical or random coil with ~20% in β-sheets. Therefore, while there is some uncertainty in distinguishing the true relative abundances of helical vs. random coil structures, both Leu Cβ and Cα deconvolution results indicate ~80% of Leu is either helical or unstructured where α-helices are dominant, and the remaining 20% of Leu exists in a β-sheet environment. The decrease in helical content from DSSP quantification (~81% helical and no β-sheets from AlphaFold model) to SSNMR (~50% helical, 30% random coil, 20% β-sheets) data certainly points to some minor conversion of bead-derived helices to β-sheets in the solid fiber. However, for the most part Leu α-helical structure is maintained from AC silk dope in the gland (**Figure 5**) through the solidified AC silk fiber.

Glycine

A broad asymmetric ^{13}C Gly CO resonance has been observed in the 2D ^{13}C SSNMR spectra of *N. clavipes* MA silk that corresponds to Gly in both β-sheet domains and 3_1-helical conformations. This has been ascribed to nanocrystalline poly(Gly-Ala) and disordered Gly-Gly-X (X = Gln, Tyr, Leu, Arg) regions found in MA silk, respectively.[41, 44, 49-51] AC silk, however, lack these regions, with most Gly being present in short linkers in the bead and the long unstructured "string" in **Figure 3** (**Table 2**). In AcSp1, the Gly is predominantly present in the unstructured long "string" domains where they are commonly flanked by Ser-rich and Ala-Ser motifs which are known to form β-sheets in the solid AC fiber including GSASG, ASSGG, and SGASAG motifs.[9]

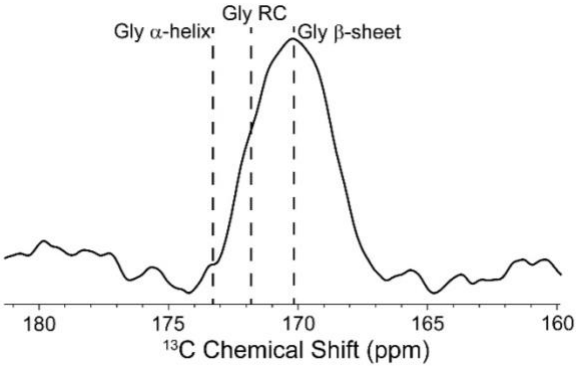

Figure 9. 215.6 ppm slice from the INADEQUATE spectrum in **Figure 7** shows Gly CO chemical shift. Typical carbonyl chemical shifts observed for different conformations are indicated with dashed lines.

A pseudo-1D spectrum produced by selecting the slice corresponding to Gly signal from the INADEQUATE experiment (**Figure 9**) was used to further characterize Gly secondary structure in AC silk. The Gly CO exhibits a narrow linewidth for the carbonyl signal with a full width at half maximum (FWHM) of 530 Hz, compared to a FWHM of 1100 Hz for the Gly carbonyl signal in *N. clavipes* MA silk, where Gly is found in multiple conformations.[41] **Figure 9** makes clear that Gly is not present in α-helical structures in AC silk fibers. A comparison of the chemical shifts to literature values also indicates that Gly is primarily present in β-sheet domains (**Table 4**). This supports the idea that much of the Gly in the random coil "string" regions in solution (dope) are converted to β-sheet structures in AC silk fibers. Close inspection of the Gly CO reveals that while no α-helical component is observed, some Gly still remains random coil as

evidenced by the high ppm shoulder. This could be due to Gly in short linker domains within the "bead" and/or incomplete conversion of the longer string to β-sheet structure. Nonetheless, Gly dominant secondary structure in AC fibers is clealry β-sheet.

Phenylalanine/Tyrosine

Phe is 3.8% abundant in the AcSp1 protein and has not previously been studied in AC silks. In dragline silk fibers, it is known that Tyr is found in disordered helical structures and not incorporated in β-sheet domains, with evidence that aromatic sidechains undergo side chain interactions.[52, 53] ^{13}C-^{13}C correlation experiments were conducted for the U-[$^{13}C/^{15}N$]-enriched Phe, Ala, and Ser (FAS) AC silk fibers (**Figure 10**) to investigate the secondary structure of aromatic amino acids in AC silk.

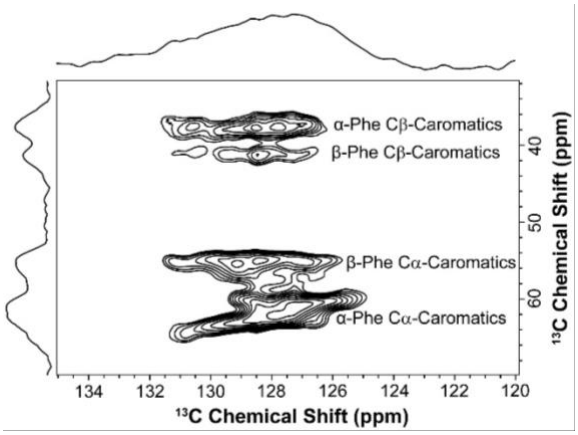

Figure 10. 2D ^{13}C-^{13}C through-space correlation DARR experiment for *A. argentata* AC silk where the spider was fed a U-[$^{13}C/^{15}N$]-enriched solution of Phe, Ala, and Ser (FAS). This experiment was conducted at a mixing time of 100 ms to see intramolecular contacts in the aromatic region of the spectrum.

In AcSp1, Phe is frequently flanked by short poly(Ser) motifs, even in the predominantly α–helical "bead" with 20 instances of SSFLS and 16 of AFSS in the "bead". In the disordered, β-sheet forming "linker" regions, there are 18 instances of SFSS and 20 instances SSFG motifs. The remaining Phe present in the protein sequence are found evenly distributed in the "bead" and "linker", with 11 of them in the termini. It is known that feeding spiders Phe metabolizes and labels Tyr,[52] which is also present in AcSp1 with 1.5% abundance. Tyr is present 39 times in GYT motifs in the unstructured "linker" region and 20 times in a AYA motif in the "bead", with 6 in the termini. Due to both Phe and Tyr being labeled by the FAS feeding scheme, the similarity in their chemical shifts (**Table 4**) and their

similar locations in the AcSp1 protein, we are unable to distinguish between the two amino acids in the SSNMR experiments conducted here. However, because the Phe is 2.5 times more abundant in AcSp1 the interpretation will be skewed more toward understanding Phe structure with the understanding that Tyr contributions cannot be discounted.

The AC silk 2D ^{13}C-^{13}C DARR spectrum (FAS-label) was too crowded in the alkyl region to resolve the signals corresponding to Cα and Cβ of the aromatic residues (Phe and Tyr) that are most sensitive to secondary structure. A close inspection of the aromatic region around 133 ppm shows only the aromatic residues Phe/Tyr (**Figure 10**), allowing us to indirectly observe the aromatic residues' Cα and Cβ chemical shifts. **Figure 10** shows two clear conformations present in Cα and Cβ, one α-helical and one β-sheet based on the chemical shifts (**Table 4**). Both chemical shifts corresponding to the helical conformation are a bit more intense, indicating a preference for the α-helix secondary structure in the fiber. Overall, however, the nearly equal representation of Phe/Tyr in the α-helical "bead" and β-sheet forming "string" domain is consistent with strong signals observed for both β-sheet and α-helical components. It should be noted that random coil contributions although not distinctively resolved, are likely also present.

2.4 SSNMR on *A. aurantia* AC Silks (Threonine)

The Basic Local Alignment Search Tool (BLAST)[54, 55] was used to compare the sequences of *A. argentata* AcSp1 and the longest known, non-terminal, sequence of *A. aurantia* AcSp1.[11] This comparison (**Figures S5, S6)** shows only 15 additional or different residues in the *A. argentata* sequence compared to the largest sequenced fragment (only 175 residues) of the *A. aurantia* sequence. Additionally, when the *A. aurantia* portion is compared to the entire *A. argentata* sequence, the fragment (or one very similar to it) is repeated 20 times, the same

number of repeating units in the entire *A. argentata* sequence. For these reasons, we consider AcSp1 from these two species identical for the purposes of our NMR structural analysis.

The seven helices that are found within the "bead" are connected by short unstructured regions (**Figure 3**), in which Thr is frequently found, although there are no consistent Thr-containing motifs in either *A. argentata* or *A. aurantia*. Thr is also present in the larger, Ala/Ser/Gly-rich longer "string" linker regions. DSSP quantification indicates a nearly even mix between helical and random coil secondary structures in the solution phase AcSp1 AlphaFold model. This indicates that these smaller linkers within the "bead" may be part of the helices or unstructured in solution.

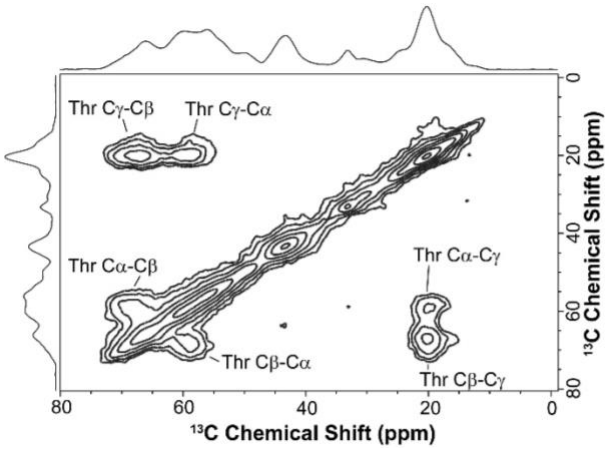

Figure 11. 2D ^{13}C-^{13}C through-space correlation DARR experiment for *A. aurantia* prey-wrap silk where the spider was fed a U-[^{13}C/^{15}N]-enriched solution of Thr with unlabeled Ala, Gly, Val, Ser, and Phe. This experiment was conducted at a mixing time of 100 ms to see intramolecular contacts.

^{13}C-^{13}C correlation experiments were conducted on Thr isotope labeled *A. aurantia* AC silk fibers to try to further elucidate its secondary structure in fibers. While being fed ^{13}C/^{15}N-labeled Thr, *A. aurantia* spiders were also fed unlabeled Ala, Gly, Val, Ser, and Phe to suppress unwanted signals from these common amino acids in AC silk. The DARR experiment conducted on this sample (**Figure 11**) shows only correlations between Thr sites, providing strong evidence that feeding spiders unlabeled amino acids can help reduce unwanted signals. A comparison of Thr chemical shifts to literature values (**Table 4**) indicates a preference for the random coil conformation, with chemical shifts in between the β-sheet and α-helical secondary structures. This is consistent with our prediction that some Thr forms helices in the helical bundle, some Thr is located at the ends of helical domains

and is mainly unstructured, and some Thr is present in the longer "strings" which could form β-sheets or remain unstructured in fibers. Perhaps not surprisingly, Thr's ubiquitous presence in the various domains of AcSp1 leads to ambiguous results due to a high degree of heterogeneity.

3. Conclusions

Mechanical tensile fiber testing confirmed the high extensibility and toughness of AC silks compared to the more commonly studied MA spider silks. The combination of the AlphaFold predicted structure of *A. argentata* AcSp1, solution-state NMR on intact glands, and SSNMR data on as-spun fibers has allowed us to update the structural model of prey-wrapping silk and gives us more insight into the AC silk assembly. Solution NMR of isotopically enriched AC glands was conducted for the first time and the results confirmed the "beads-on-string" model where chemical shift trends tracked with α-helical content determined from the AlphaFold model. The solution NMR data in the AC silk gland showed that Leu was predominantly α-helical, Val and Ala leaned towards helical while, Gly was shown to be almost exclusively random coil consistent with its dominant location in "string" domains. In-depth SSNMR data was used to further understand the conformational structure of Pro, Leu, Gly, Thr, and Phe/Tyr within the post-spun AC fiber. Pro takes on an elastin-like type-II β-turn conformation in AC silk fibers, a conformation that is not found in the glands. This conformation is consistent with previously observed Pro-containing regions of dragline spider silk. Leucine has a strong preference for the α-helical conformation in both the gland and the solid fiber, with evidence of a slight conversion of some helical content to β-sheet in the fiber. Gly is predominantly in a β-sheet structure in the Ala/Ser-rich "string" regions of AC silk fibers, while it is in a disordered random coil structure in solution (dope phase). Thr appears to be unstructured in the fiber, with evidence that it forms some β-sheets and α-helices. The Thr labeled *A. aurantia* sample also

provides strong evidence that feeding spiders unlabeled amino acids can help reduce unwanted SSNMR signals in labeled natural silk fibers.

The generally high helical content of the AC silk protein in solution, shown in the DSSP quantification derived from the AlphaFold model of AcSp1 is consistent with the impressive extensibility of AC silks. The greater presence of the β-sheet conformation in solid fibers compared to the gland, which is shown in the SSNMR data, is consistent with the conversion of disordered regions in solution to β-sheets in the silk fibers. It's interesting that Leu appears marginally less helical with more disordered and β-sheet content compared to Val as previously described, even though we expected Val and Leu to be structurally similar. We have previously noticed a hydration-induced α to β structural transition in wrapping silks, and other coiled-coil polymers like Keratin demonstrate α to β transition on elongation.[35] It therefore seems likely that prey-wrapping silks are highly helical on initial fiber formation but are dynamically structured and undergo similar α to β transition on stretching and/or hydration. This is being explored in the lab currently and will be published in a future study. The ability of AC to form β-sheets upon stretching-related unraveling of helices likely contributes to the remarkable toughness of AC silks shown by mechanical testing. The conserved α-helices in the solid fiber, on the other hand, contribute to the extensibility of AC silks.

4. Experimental Section

AC Silk Collection and Isotope Labeling for NMR. Adult female *A. argentata* spiders had their AC silks isotopically enriched by being fed U-[^{13}C/^{15}N]-enriched amino acids dissolved in water every other day over the course of two weeks. The amino acid solution concentrations were based approximately on their solubility limit in 1 mL of water.[56] One group of spiders were fed an amino acid solution of U-[^{13}C/^{15}N]-enriched Val, Ala, Leu, and Pro (VALP) and AC silk was

collected. A second group of *A. argentata* spiders were fed an amino acid solution of U-[^{13}C/^{15}N]-enriched Phe, Ala, and Ser (FAS). And, a third group of *A. aurantia* spiders were similarly fed an amino acid solution of U-[^{13}C/^{15}N]-enriched Thr with unlabeled Ala, Gly, Val, Ser, and Phe. The feeding of unlabeled amino acids minimizes the scrambling of isotopes resulting in more selective isotope labeling. Spiders were also fed one cricket per week. Prey-wrapping (AC) silk was collected by vibration induced attack wrapping as described previously.[9, 57] AC silk fiber samples were transferred to MAS rotors for SSNMR.

Isotope labeled AC silk gland samples for solution NMR were produced similar to the SSNMR samples. Four different solution NMR AC silk gland samples were prepared as follows. Over two weeks, AC silk was collected by attack wrapping from *A. aurantia* spiders every other day while feeding solutions containing U-[^{13}C/^{15}N]-enriched amino acids. Spiders were separated into four different groups - one group was fed U-[^{13}C/^{15}N]-enriched Leu alongside unlabeled Ala, Gly, Val, Ser, and Phe – a second group was fed U-[^{13}C/^{15}N]-enriched Val with unlabeled Phe – a third group was fed U-[^{13}C/^{15}N]-Thr with unlabeled Ala, Gly, Val, Ser, and Phe – a fourth group was fed U-[^{13}C/^{15}N]-Ala with unlabeled Phe.

Silk Mechanical Testing. A KeySight UTM T150 mechanical testing system was used to measure the tensile properties of silks from three different species of spiders, *N. clavipes*, *L. hesperus*, and *A. argentata*. Spiders were anesthetized with CO_2 and restrained on their back with pieces of masking tape. Mechanical testing was performed as close as possible to the method described by Blackledge et al.[27] Dragline (MA) fibers from different spiders were forcibly silked at a rate of 1.5 cm/s ensuring that only MA silk was collected by separating the minor (MI) ampullate strands. To ensure our tests were single-fiber measurements we used a needle to gently break all but a single fiber. While silking, pieces of cardstock with rectangular cutouts were placed underneath the extended fibers. Acrylic glue was then used to secure the strand of silk in place on

either side of the cutouts. To ensure our tests were single-fiber measurements, the carboard cutouts were placed under a microscope at 500X magnification to ensure single fibers were present rather than bundles. These cardboard cutouts were then placed vertically in the tensile tester and an increasing load was placed on the fibers such that they were strained at 1% per second until failure. Silk fiber diameters were measured with an optical microscope with the exception of AC silk which was measured with SEM and found to consistently show 0.5 μm diameters. Prey-wrapping (AC) silks were obtained by inducing *A. argentata* spiders to "attack-wrap" an electric toothbrush. Similar cutouts as above were then placed between the spider and the toothbrush until a swath of silk was wrapped around the card. Then using a fine needle, fiber swaths were thinned down to a single fiber and then glued in place as above.

SEM. Prey wrap (AC) silk was mounted to SEM sample stubs using carbon tape [58]and coated in 6 nm of platinum using an EMS 150 sputter coater. Samples were imaged at SDSU's electron microscope facility using an FEI Quanta 450 FEG Scanning Electron Microscope at 10 kV, spot size 3.5 with a secondary electron detector.

Solution NMR. Unlike the much more commonly studied MA glands, AC glands are not paired and are much smaller and harder to locate and excise. AC silk glands were identified by their distinct "finger-like" morphology and were dissected from adult female *A. aurantia* spiders using previously described methods as a guide.[58, 59] Intact AC glands were transferred into 5mm Shigemi tubes filled with 90:10 H_2O:D_2O and 1mM DSS for referencing (**Figure S7**). Experiments were conducted at 600 MHz with an Avance III HD Bruker NMR spectrometer and TXI solution probe. 2D HSQC experiments were performed using both ^{1}H-^{13}C and ^{1}H-^{15}N HSQC experiments for isotope-enriched AC silk glands. ^{1}H-^{13}C experiments were collected

using 2048x512 points and 16 scans. ^{1}H-^{15}N experiments were collected with 2048x256 points and 64 scans. The recycle delay (d1) was 2s and all chemical shifts are referenced to DSS.

Solid-State NMR. Experiments were performed using a 600 MHz (14.1 Tesla) Bruker AVANCE-IIIHD spectrometer equipped with a Bruker 1.9 mm HCN MAS probe or using a 500 MHz (11.7 Tesla) Varian VNMRS spectrometer equipped with a Phoenix 1.6 mm HXY MAS probe. 2D DARR experiments[41, 42, 52, 60, 61] for isotope-enriched *A. aurantia* silks were conducted on the Varian spectrometer with MAS spinning of 20 kHz and collected with 128 scans and 128 t1 points. The proton 90° pulse length was 2 μs. A CP contact time of 1.5 ms was used. Carbon 90° pulse length was 2.5 μs. DARR mixing time of 100 ms and TPPM ^{1}H decoupling with a 92 kHz rf field strength during acquisition with an 11° phase shift. The recycle delay was 4 s. Refocused INADEQUATE experiments[42, 43, 52, 62] were performed on the Bruker spectrometer with MAS spinning at 30 kHz and collected with 512 scans and 196 t1 points. The proton 90° pulse length was 2.5 μs. A CP contact time of 2 ms was used. Carbon 90° and 180° pulse lengths of 2.5 and 5.0 μs, respectively. The τ delay was 3.5 ms. SWFTPPM ^{1}H decoupling with a 125 kHz rf field strength was applied throughout the entire pulse sequence and during acquisition with a 13° phase shift. The recycle delay was 2.5 s.

Quantitative ^{13}C 1D SSNMR (Direct and with MultiCP) and 2D through-space ^{13}C-^{13}C correlation experiments were collected on a 600 MHz (14.1 Tesla) Bruker NEO NMR spectrometer equipped with a Phoenix 1.6 mm probe (Loveland, CO) operating in double resonance mode with 10 kHz MAS. Quantitative MultiCP[63] data were collected with 4096 scan averages, 2.5 μs hard pulses for both ^{1}H and ^{13}C, and the MultiCP block was performed using a total of eight 1.1 ms CP blocks (square 62 kHz spin-lock on ^{13}C, 14% ramped spin-lock step on ^{1}H matched to the +1 sideband) separated by 0.8 second t_z repolarization delays, and a recycle

delay of 0.5 seconds. An additional ^{13}C storage pulse and 20 ms z-filter was applied before detection to further equilibrate ^{13}C magnetization,[64] and a rotor synchronized Hahn echo was also applied to achieve a clean baseline. Quantitative conditions were verified by comparing the resulting CP-MAS spectrum to MultiCP spectrum to a fully relaxed ^{13}C spectrum (DP-MAS, 60 second recycle delay) (**Figure S8**). 2D CORD spectra were collected with 256 scan averages and 320 indirect points, 50 kHz and 30 kHz sweep widths in the direct and indirect dimensions, and with mixing times of 50 and 500 ms. ^{1}H dipolar coupling was reintroduced using a CORD recoupling scheme.[36] Hard pulses were 2.5 μs for both ^{1}H and ^{13}C, and CP was achieved using a square 2 ms 62.5 kHz spin locking pulse on the ^{13}C channel and a 14% ramped pulse on the ^{1}H channel matched to the +1 sideband. 125 kHz high power proton decoupling was applied during acquisition for all experiments (Bruker sequence swftppm13). 2D through-space spin-diffusion data were typically processed with MestreNova using 20 Hz exponential line broadening in the direct dimension and with a 90° shifted sine bell apodization in the indirect dimension. Spectral deconvolution was performed by first extracting initial guesses for peak positions and linewidths from 2D data, then fitting the extracted 1D spectrum using custom python code using the lmfit module.[65]

All ^{13}C chemical shifts were referenced externally to TMS at 0.0 ppm by setting the downfield adamantane signal to 38.48 ppm.[66]

AlphaFold Modeling and Secondary Structure Quantification. AcSp structural model was generated using AlphaFold2[25, 26] to predict the structure from the AC silk protein primary amino acid sequence. Utilizing the secondary structure assignment built in PyMol, amino acids were defined as either helical or unstructured. Amino acid assignments were used to update the "beads-on-a-string" model to define the helical portions within the "bead" as well as the

unstructured “string”. The 4479 amino acid *A. argentata* AcSp1 (**Figure S1**) (UniProt: W8FUS3) was split into 6 portions (630, 816, 816, 816, 816, and 585 amino acids) for AlphaFold structural predictions to look at the complete sequence piecemeal (**Figure 3**). These individual structures were passed to DSSP, an algorithm for secondary structure assignment of proteins.[67] DSSP results for each predicted AlphaFold structure were appended for secondary structure quantification of the full 4479 amino acids (**Table S1**).

Protein-protein BLAST sequence alignment was performed on *A. argentata* AcSp1 (UniProt: W8FUS3) against *A. aurantia* AcSp1 (Uniprot: W8FM39) using default search parameters.[54, 55]

Acknowledgements

This work was supported by the Department of Defense Army Research Office (DOD-ARO) under grant contract No. W911NF2410099 (G.P.H.). B.A. was supported by the National Renewable Energy Laboratory, operated by Alliance for Sustainable Energy, LLC for the U.S. Department of Energy. This work was supported by the U.S. Department of Energy, Office of Science, Office of Biological and Environmental Research, Genomic Science Program under Secure Biosystems Design Science Focus Area IMAGINE BioSecurity: Integrative Modeling and Genome-scale Engineering for Biosystems Security under contract no. DE-AC36-08GO28308. The views expressed in the article do not necessarily represent the views of the DOE or the U.S. Government. The U.S. Government retains, and the publisher, by accepting the article for publication, acknowledges that the U.S. Government retains a nonexclusive, paid-up, irrevocable, worldwide license to publish or reproduce the published form of this work, or allow others to do so, for U.S. Government purposes. The authors also gratefully acknowledge extensive discussion with Prof. Cheryl Hayashi regarding AC silk gland dissection.

Table of Contents

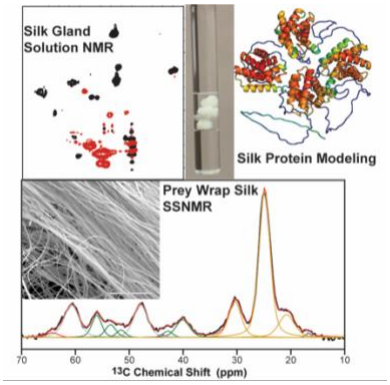

Prey wrap silk exhibits a high extensibility and superior toughness compared to other types of spider silk. Solution NMR of intact silk glands and solid-state NMR of solid fibers were performed to elucidate the silk's unique liquid-to-solid transition. These results and models will provide the basis for the design of biomimetic materials inspired by the prey wrap spider silk system.

References

(1) Eisoldt, L.; Smith, A.; Scheibel, T. Decoding the secrets of spider silk. *Materials Today* **2011**, *14* (3), 80-86. DOI: https://doi.org/10.1016/S1369-7021(11)70057-8.
(2) Römer, L.; Scheibel, T. The elaborate structure of spider silk: structure and function of a natural high performance fiber. *Prion* **2008**, *2* (4), 154-161. DOI: 10.4161/pri.2.4.7490 From NLM.
(3) Bakhshandeh, B.; Nateghi, S. S.; Gazani, M. M.; Dehghani, Z.; Mohammadzadeh, F. A review on advances in the applications of spider silk in biomedical issues. *International Journal of Biological Macromolecules* **2021**, *192*, 258-271. DOI: https://doi.org/10.1016/j.ijbiomac.2021.09.201.
(4) Yarger, J. L.; Cherry, B. R.; van der Vaart, A. Uncovering the structure–function relationship in spider silk. *Nature Reviews Materials* **2018**, *3* (3), 18008. DOI: 10.1038/natrevmats.2018.8.
(5) Lewis, R. V. Spider Silk: Ancient Ideas for New Biomaterials. *Chemical Reviews* **2006**, *106* (9), 3762-3774. DOI: 10.1021/cr010194g.
(6) Hayashi, C. Y.; Blackledge, T. A.; Lewis, R. V. Molecular and Mechanical Characterization of Aciniform Silk: Uniformity of Iterated Sequence Modules in a Novel Member of the Spider Silk Fibroin Gene Family. *Molecular Biology and Evolution* **2004**, *21* (10), 1950-1959. DOI: 10.1093/molbev/msh204 (acccessed 9/26/2023).
(7) Bailey, A. J.; Macmillan, J.; Shrewry, P. R.; Tatham, A. S.; Gosline, J.; Lillie, M.; Carrington, E.; Guerette, P.; Ortlepp, C.; Savage, K. Elastic proteins: biological roles and mechanical properties. *Philosophical Transactions of the Royal Society of London. Series B: Biological Sciences* **2002**, *357* (1418), 121-132. DOI: doi:10.1098/rstb.2001.1022.
(8) Blackledge, T. A.; Hayashi, C. Y. Silken toolkits: biomechanics of silk fibers spun by the orb web spider Argiope argentata (Fabricius 1775). *J Exp Biol* **2006**, *209* (Pt 13), 2452-2461. DOI: 10.1242/jeb.02275 From NLM.
(9) Addison, B.; Onofrei, D.; Stengel, D.; Blass, B.; Brenneman, B.; Ayon, J.; Holland, G. P. Spider prey-wrapping silk is an α-helical coiled-coil/β-sheet hybrid nanofiber. *Chemical Communications* **2018**, *54* (76), 10746-10749, 10.1039/C8CC05246H. DOI: 10.1039/C8CC05246H.
(10) Stengel, D.; Addison, J. B.; Onofrei, D.; Huynh, N. U.; Youssef, G.; Holland, G. P. Hydration-Induced β-Sheet Crosslinking of α-Helical-Rich Spider Prey-Wrapping Silk. *Advanced Functional Materials* **2021**, *31* (13), 2007161. DOI: https://doi.org/10.1002/adfm.202007161.
(11) Chaw, R. C.; Zhao, Y.; Wei, J.; Ayoub, N. A.; Allen, R.; Atrushi, K.; Hayashi, C. Y. Intragenic homogenization and multiple copies of prey-wrapping silk genes in Argiopegarden spiders. *BMC Evolutionary Biology* **2014**, *14* (1), 31. DOI: 10.1186/1471-2148-14-31.

(12) Xu, L.; Tremblay, M.-L.; Meng, Q.; Liu, X.-Q.; Rainey, J. K. 1H, 13C and 15N NMR assignments of the aciniform spidroin (AcSp1) repetitive domain of Argiope trifasciata wrapping silk. *Biomolecular NMR Assignments* **2012**, *6* (2), 147-151. DOI: 10.1007/s12104-011-9344-z.
(13) Tremblay, M.-L.; Xu, L.; Lefèvre, T.; Sarker, M.; Orrell, K. E.; Leclerc, J.; Meng, Q.; Pézolet, M.; Auger, M.; Liu, X.-Q.; Rainey, J. K. Spider wrapping silk fibre architecture arising from its modular soluble protein precursor. *Scientific Reports* **2015**, *5* (1), 11502. DOI: 10.1038/srep11502.
(14) Sarker, M.; Orrell, K. E.; Xu, L.; Tremblay, M.-L.; Bak, J. J.; Liu, X.-Q.; Rainey, J. K. Tracking Transitions in Spider Wrapping Silk Conformation and Dynamics by 19F Nuclear Magnetic Resonance Spectroscopy. *Biochemistry* **2016**, *55* (21), 3048-3059. DOI: 10.1021/acs.biochem.6b00429.
(15) Tremblay, M.-L.; Xu, L.; Sarker, M.; Liu, X.-Q.; Rainey, J. K. Characterizing Aciniform Silk Repetitive Domain Backbone Dynamics and Hydrodynamic Modularity. *International Journal of Molecular Sciences* **2016**, *17* (8), 1305.
(16) Parent, L. R.; Onofrei, D.; Xu, D.; Stengel, D.; Roehling, J. D.; Addison, J. B.; Forman, C.; Amin, S. A.; Cherry, B. R.; Yarger, J. L.; Gianneschi, N. C.; Holland, G. P. Hierarchical spidroin micellar nanoparticles as the fundamental precursors of spider silks. *Proceedings of the National Academy of Sciences* **2018**, *115* (45), 11507-11512. DOI: doi:10.1073/pnas.1810203115.
(17) Hijirida, D. H.; Do, K. G.; Michal, C.; Wong, S.; Zax, D.; Jelinski, L. W. 13C NMR of Nephila clavipes major ampullate silk gland. *Biophys J* **1996**, *71* (6), 3442-3447. DOI: 10.1016/s0006-3495(96)79539-5 From NLM.
(18) Hronska, M.; van Beek, J. D.; Williamson, P. T.; Vollrath, F.; Meier, B. H. NMR characterization of native liquid spider dragline silk from Nephila edulis. *Biomacromolecules* **2004**, *5* (3), 834-839. DOI: 10.1021/bm0343904 From NLM.
(19) Xu, D.; Yarger, J. L.; Holland, G. P. Exploring the backbone dynamics of native spider silk proteins in Black Widow silk glands with solution-state NMR spectroscopy. *Polymer* **2014**, *55* (16), 3879-3885. DOI: https://doi.org/10.1016/j.polymer.2014.06.018.
(20) Onofrei, D.; Stengel, D.; Jia, D.; Johnson, H. R.; Trescott, S.; Soni, A.; Addison, B.; Muthukumar, M.; Holland, G. P. Investigating the Atomic and Mesoscale Interactions that Facilitate Spider Silk Protein Pre-Assembly. *Biomacromolecules* **2021**, *22* (8), 3377-3385. DOI: 10.1021/acs.biomac.1c00473.
(21) Jenkins, J. E.; Holland, G. P.; Yarger, J. L. High resolution magic angle spinning NMR investigation of silk protein structure within major ampullate glands of orb weaving spiders. *Soft Matter* **2012**, *8* (6), 1947-1954, 10.1039/C2SM06462F. DOI: 10.1039/C2SM06462F.
(22) Xu, L.; Rainey, J. K.; Meng, Q.; Liu, X.-Q. Recombinant Minimalist Spider Wrapping Silk Proteins Capable of Native-Like Fiber Formation. *PLOS ONE* **2012**, *7* (11), e50227. DOI: 10.1371/journal.pone.0050227.
(23) Xu, L.; Lefèvre, T.; Orrell, K. E.; Meng, Q.; Auger, M.; Liu, X.-Q.; Rainey, J. K. Structural and Mechanical Roles for the C-Terminal Nonrepetitive Domain Become Apparent in Recombinant Spider Aciniform Silk. *Biomacromolecules* **2017**, *18* (11), 3678-3686. DOI: 10.1021/acs.biomac.7b01057.
(24) Xu, L.; Weatherbee-Martin, N.; Liu, X.-Q.; Rainey, J. K. Recombinant Silk Fiber Properties Correlate to Prefibrillar Self-Assembly. *Small* **2019**, *15* (12), 1805294. DOI: https://doi.org/10.1002/smll.201805294.
(25) Jumper, J.; Evans, R.; Pritzel, A.; Green, T.; Figurnov, M.; Ronneberger, O.; Tunyasuvunakool, K.; Bates, R.; Žídek, A.; Potapenko, A.; Bridgland, A.; Meyer, C.; Kohl, S. A. A.; Ballard, A. J.; Cowie, A.; Romera-Paredes, B.; Nikolov, S.; Jain, R.; Adler, J.; Back, T.; Petersen, S.; Reiman, D.; Clancy, E.; Zielinski, M.; Steinegger, M.; Pacholska, M.; Berghammer, T.; Bodenstein, S.; Silver, D.; Vinyals, O.; Senior, A. W.; Kavukcuoglu, K.; Kohli, P.; Hassabis, D. Highly accurate protein structure prediction with AlphaFold. *Nature* **2021**, *596* (7873), 583-589. DOI: 10.1038/s41586-021-03819-2.
(26) Varadi, M.; Anyango, S.; Deshpande, M.; Nair, S.; Natassia, C.; Yordanova, G.; Yuan, D.; Stroe, O.; Wood, G.; Laydon, A.; Žídek, A.; Green, T.; Tunyasuvunakool, K.; Petersen, S.; Jumper, J.; Clancy, E.; Green, R.; Vora, A.; Lutfi, M.; Figurnov, M.; Cowie, A.; Hobbs, N.; Kohli, P.; Kleywegt, G.; Birney, E.; Hassabis, D.; Velankar, S. AlphaFold Protein Structure Database: massively expanding the structural

coverage of protein-sequence space with high-accuracy models. *Nucleic Acids Research* **2021**, *50* (D1), D439-D444. DOI: 10.1093/nar/gkab1061 (acccessed 9/27/2023).
(27) Blackledge, T. A.; Swindeman, J. E.; Hayashi, C. Y. Quasistatic and continuous dynamic characterization of the mechanical properties of silk from the cobweb of the black widow spider Latrodectus hesperus. *Journal of Experimental Biology* **2005**, *208* (10), 1937-1949. DOI: 10.1242/jeb.01597 (acccessed 5/14/2024).
(28) Gosline, J. M.; Guerette, P. A.; Ortlepp, C. S.; Savage, K. N. The mechanical design of spider silks: from fibroin sequence to mechanical function. *Journal of Experimental Biology* **1999**, *202* (23), 3295.
(29) Blackledge, T. A.; Zevenbergen, J. M. Condition-dependent spider web architecture in the western black widow, Latrodectus hesperus. *Anim. Behav.* **2007**, *73* (5), 855-864. DOI: https://doi.org/10.1016/j.anbehav.2006.10.014.
(30) Madsen, B.; Shao, Z. Z.; Vollrath, F. Variability in the mechanical properties of spider silks on three levels: interspecific, intraspecific and intraindividual. *Int J Biol Macromol* **1999**, *24* (2-3), 301-306. DOI: 10.1016/S0141-8130(98)00094-4.
(31) Swanson, B. O.; Blackledge, T. A.; Beltran, J.; Hayashi, C. Y. Variation in the material properties of spider dragline silk across species. *Appl. Phys. A: Mater. Sci. Process.* **2006**, *82*, 213-218. DOI: 10.1007/s00339-005-3427-6.
(32) Madurga, R.; Plaza, G. R.; Blackledge, T. A.; Guinea, G. V.; Elices, M.; Pérez-Rigueiro, J. Material properties of evolutionary diverse spider silks described by variation in a single structural parameter. *Sci. Rep.* **2016**, *6* (1), 18991-18991. DOI: 10.1038/srep18991.
(33) Agnarsson, I.; Kuntner, M.; Blackledge, T. A. Bioprospecting finds the toughest biological material: extraordinary silk from a giant riverine orb spider. *PLoS One* **2010**, *5* (9), e11234. DOI: 10.1371/journal.pone.0011234.
(34) Wang, Y.; Jardetzky, O. Probability-based protein secondary structure identification using combined NMR chemical-shift data. *Protein Sci* **2002**, *11* (4), 852-861. DOI: 10.1110/ps.3180102 From NLM.
(35) Kreplak, L.; Doucet, J.; Dumas, P.; Briki, F. New aspects of the alpha-helix to beta-sheet transition in stretched hard alpha-keratin fibers. *Biophys J* **2004**, *87* (1), 640-647. DOI: 10.1529/biophysj.103.036749 From NLM Medline.
(36) Hou, G.; Yan, S.; Trébosc, J.; Amoureux, J. P.; Polenova, T. Broadband homonuclear correlation spectroscopy driven by combined R2(n)(v) sequences under fast magic angle spinning for NMR structural analysis of organic and biological solids. *J Magn Reson* **2013**, *232*, 18-30. DOI: 10.1016/j.jmr.2013.04.009 From NLM.
(37) Kricheldorf, H. R.; Müller, D. Secondary structure of peptides: 15. 13C n.m.r. CP/MAS study of solid elastin and proline-containing copolyesters. *International Journal of Biological Macromolecules* **1984**, *6* (3), 145-151. DOI: https://doi.org/10.1016/0141-8130(84)90056-4.
(38) Saitô, H.; Tabeta, R.; Shoji, A.; Ozaki, T.; Ando, I.; Miyata, T. A high-resolution 13C-NMR study of collagenlike polypeptides and collagen fibrils in solid state studied by the cross-polarization–magic angle-spinning method. Manifestation of conformation-dependent 13C chemical shifts and application to conformational characterization. *Biopolymers* **1984**, *23* (11), 2279-2297. DOI: https://doi.org/10.1002/bip.360231111.
(39) Ohgo, K.; Ashida, J.; Kumashiro, K. K.; Asakura, T. Structural Determination of an Elastin-Mimetic Model Peptide, (Val-Pro-Gly-Val-Gly)6, Studied by 13C CP/MAS NMR Chemical Shifts, Two-Dimensional off Magic Angle Spinning Spin-Diffusion NMR, Rotational Echo Double Resonance, and Statistical Distribution of Torsion Angles from Protein Data Bank. *Macromolecules* **2005**, *38* (14), 6038-6047. DOI: 10.1021/ma050052e.
(40) Bundi, A.; Wüthrich, K. 1H-NMR parameters of the common amino acid residues measured in aqueous solutions of the linear tetrapeptides H-Gly-Gly-X-L-Ala-OH. *Biopolymers* **1979**, *18* (2), 285-297. DOI: https://doi.org/10.1002/bip.1979.360180206.
(41) Holland, G. P.; Creager, M. S.; Jenkins, J. E.; Lewis, R. V.; Yarger, J. L. Determining Secondary Structure in Spider Dragline Silk by Carbon−Carbon Correlation Solid-State NMR Spectroscopy. *Journal of the American Chemical Society* **2008**, *130* (30), 9871-9877. DOI: 10.1021/ja8021208.

(42) Jenkins, J. E.; Creager, M. S.; Butler, E. B.; Lewis, R. V.; Yarger, J. L.; Holland, G. P. Solid-State NMR Evidence for Elastin-Like β-Turn Structure in Spider Dragline Silk. *Chemical Communications* **2010**, *46* (36), 6714-6716, 10.1039/C0CC00829J. DOI: 10.1039/C0CC00829J.
(43) Holland, G. P.; Jenkins, J. E.; Creager, M. S.; Lewis, R. V.; Yarger, J. L. Quantifying the Fraction of Glycine and Alanine in β-sheet and Helical Conformations in Spider Dragline Silk using Solid-State NMR. *Chemical Communications* **2008**, (43), 5568-5570, 10.1039/B812928B. DOI: 10.1039/B812928B.
(44) van Beek, J. D.; Hess, S.; Vollrath, F.; Meier, B. H. The Molecular Structure of Spider Dragline Silk: Folding and Orientation of the Protein Backbone. *Proceedings of the National Academy of Sciences* **2002**, *99* (16), 10266-10271. DOI: doi:10.1073/pnas.152162299.
(45) Liu, Y.; Shao, Z.; Vollrath, F. Elasticity of Spider Silks. *Biomacromolecules* **2008**, *9* (7), 1782-1786. DOI: 10.1021/bm7014174.
(46) Liu, Y.; Sponner, A.; Porter, D.; Vollrath, F. Proline and Processing of Spider Silks. *Biomacromolecules* **2008**, *9* (1), 116-121. DOI: 10.1021/bm700877g.
(47) Savage, K. N.; Gosline, J. M. The role of proline in the elastic mechanism of hydrated spider silks. *Journal of Experimental Biology* **2008**, *211* (12), 1948-1957. DOI: 10.1242/jeb.014225 (acccessed 5/16/2023).
(48) Fritzsching, K. J.; Yang, Y.; Schmidt-Rohr, K.; Hong, M. Practical use of chemical shift databases for protein solid-state NMR: 2D chemical shift maps and amino-acid assignment with secondary-structure information. *Journal of Biomolecular NMR* **2013**, *56* (2), 155-167. DOI: 10.1007/s10858-013-9732-z.
(49) Ayoub, N. A.; Garb, J. E.; Tinghitella, R. M.; Collin, M. A.; Hayashi, C. Y. Blueprint for a High-Performance Biomaterial: Full-Length Spider Dragline Silk Genes. *PLOS ONE* **2007**, *2* (6), e514. DOI: 10.1371/journal.pone.0000514.
(50) Jenkins, J. E.; Sampath, S.; Butler, E.; Kim, J.; Henning, R. W.; Holland, G. P.; Yarger, J. L. Characterizing the Secondary Protein Structure of Black Widow Dragline Silk Using Solid-State NMR and X-ray Diffraction. *Biomacromolecules* **2013**, *14* (10), 3472-3483. DOI: 10.1021/bm400791u.
(51) Gray, G. M.; Van der Vaart, A.; Guo, C.; Jones, J.; Onofrei, D.; Cherry, B. R.; Lewis, R. V.; Yarger, J. L.; Holland, G. P. Secondary Structure Adopted by the Gly-Gly-X Repetitive Regions of Dragline Spider Silk. *International Journal of Molecular Sciences* **2016**, *17* (12), 2023.
(52) Izdebski, T.; Akhenblit, P.; Jenkins, J. E.; Yarger, J. L.; Holland, G. P. Structure and Dynamics of Aromatic Residues in Spider Silk: 2D Carbon Correlation NMR of Dragline Fibers. *Biomacromolecules* **2010**, *11* (1), 168-174. DOI: 10.1021/bm901039e.
(53) Chalek, K.; Soni, A.; Lorenz, C. D.; Holland, G. P. Proline–Tyrosine Ring Interactions in Black Widow Dragline Silk Revealed by Solid-State Nuclear Magnetic Resonance and Molecular Dynamics Simulations. *Biomacromolecules* **2024**. DOI: 10.1021/acs.biomac.3c01351.
(54) Altschul, S. F.; Gish, W.; Miller, W.; Myers, E. W.; Lipman, D. J. Basic local alignment search tool. *J Mol Biol* **1990**, *215* (3), 403-410. DOI: 10.1016/s0022-2836(05)80360-2 From NLM.
(55) Altschul, S. F.; Madden, T. L.; Schäffer, A. A.; Zhang, J.; Zhang, Z.; Miller, W.; Lipman, D. J. Gapped BLAST and PSI-BLAST: a new generation of protein database search programs. *Nucleic Acids Res* **1997**, *25* (17), 3389-3402. DOI: 10.1093/nar/25.17.3389 From NLM.
(56) Nomoto, A.; Nishinami, S.; Shiraki, K. Solubility Parameters of Amino Acids on Liquid-Liquid Phase Separation and Aggregation of Proteins. *Front Cell Dev Biol* **2021**, *9*, 691052. DOI: 10.3389/fcell.2021.691052 From NLM.
(57) Robinson, M. H. Predatory Behavior of Argiope argentata (Fabricius). *American Zoologist* **1969**, *9* (1), 161-173. (acccessed 2023/10/02/).JSTOR.
(58) Jeffery, F.; La Mattina, C.; Tuton-Blasingame, T.; Hsia, Y.; Gnesa, E.; Zhao, L.; Franz, A.; Vierra, C. Microdissection of Black Widow Spider Silk-producing Glands. *J. Vis. Exp.* **2011**, *47*, e2382.
(59) Chaw, R. C.; Hayashi, C. Y. Dissection of silk glands in the Western black widowLatrodectus hesperus. *Journal of Arachnology* **2018**, *46* (1), 159-161. DOI: 10.1636/JoA-16-S-063.1.
(60) Takegoshi, K.; Nakamura, S.; Terao, T. 13C–1H Dipolar-Assisted Rotational Resonance in Magic-Angle Spinning NMR. *Chemical Physics Letters* **2001**, *344* (5), 631-637. DOI: https://doi.org/10.1016/S0009-2614(01)00791-6.

(61) Takegoshi, K.; Nakamura, S.; Terao, T. C13–1H Dipolar-Driven C13–13C Recoupling Without C13 RF Irradiation in Nuclear Magnetic Resonance of Rotating Solids. *The Journal of Chemical Physics* **2003**, *118* (5), 2325-2341. DOI: 10.1063/1.1534105 (acccessed 11/21/2023).
(62) Lesage, A.; Bardet, M.; Emsley, L. Through-Bond Carbon−Carbon Connectivities in Disordered Solids by NMR. *Journal of the American Chemical Society* **1999**, *121* (47), 10987-10993. DOI: 10.1021/ja992272b.
(63) Johnson, R. L.; Schmidt-Rohr, K. Quantitative solid-state 13C NMR with signal enhancement by multiple cross polarization. *Journal of Magnetic Resonance* **2014**, *239*, 44-49. DOI: https://doi.org/10.1016/j.jmr.2013.11.009.
(64) Addison, B.; Bu, L.; Bharadwaj, V.; Crowley, M. F.; Harman-Ware, A. E.; Crowley, M. F.; Bomble, Y. J.; Ciesielski, P. N. Atomistic, macromolecular model of the Populus secondary cell wall informed by solid-state NMR. *Science Advances* **2024**, *10* (1), eadi7965. DOI: doi:10.1126/sciadv.adi7965.
(65) Addison, B.; Bu, L.; Bharadwaj, V.; Crowley, M. F.; Harman-Ware, A. E.; Crowley, M. F.; Bomble, Y. J.; Ciesielski, P. N. Atomistic, macromolecular model of the Populus secondary cell wall informed by solid-state NMR. *Science Advances 10* (1), eadi7965. DOI: 10.1126/sciadv.adi7965 (acccessed 2024/05/28).
(66) Morcombe, C. R.; Zilm, K. W. Chemical shift referencing in MAS solid state NMR. *Journal of Magnetic Resonance* **2003**, *162* (2), 479-486. DOI: https://doi.org/10.1016/S1090-7807(03)00082-X.
(67) Joosten, R. P.; te Beek, T. A. H.; Krieger, E.; Hekkelman, M. L.; Hooft, R. W. W.; Schneider, R.; Sander, C.; Vriend, G. A series of PDB related databases for everyday needs. *Nucleic Acids Research* **2010**, *39* (suppl_1), D411-D419. DOI: 10.1093/nar/gkq1105 (acccessed 4/19/2024).